



HAL
open science

Controls on tetrahedral Fe(III) abundance in 2:1 phyllosilicates-Discussion

Sabine Petit, Fabien Baron, Alain Decarreau

► **To cite this version:**

Sabine Petit, Fabien Baron, Alain Decarreau. Controls on tetrahedral Fe(III) abundance in 2:1 phyllosilicates-Discussion. *The American Mineralogist*, 2021, 106 (9), pp.1534 - 1535. 10.2138/am-2021-7865 . hal-03373415

HAL Id: hal-03373415

<https://hal.science/hal-03373415>

Submitted on 11 Oct 2021

HAL is a multi-disciplinary open access archive for the deposit and dissemination of scientific research documents, whether they are published or not. The documents may come from teaching and research institutions in France or abroad, or from public or private research centers.

L'archive ouverte pluridisciplinaire **HAL**, est destinée au dépôt et à la diffusion de documents scientifiques de niveau recherche, publiés ou non, émanant des établissements d'enseignement et de recherche français ou étrangers, des laboratoires publics ou privés.

1 **Revision 1**

2 **Controls on tetrahedral Fe(III) abundance in 2:1 phyllosilicates - - Discussion**

3 PETIT SABINE*, BARON FABIEN, AND DECARREAU ALAIN

4 Institut de Chimie des Milieux et Matériaux de Poitiers (IC2MP), UMR 7285 CNRS, Université de
5 Poitiers, F-86073 Poitiers Cedex 9, France

6

7

8 Corresponding Author:

9 Sabine PETIT

10 Present address:

11 UMR 7285 CNRS, Université de Poitiers, F-86073 Poitiers Cedex 9, France.

12 *E-mail: sabine.petit@univ-poitiers.fr

13

14

15

16 **ABSTRACT**

17 Cuadros et al. (2019) used a wide range of data from dioctahedral and trioctahedral Fe³⁺-bearing
18 2:1 phyllosilicates, to propose a model describing how tetrahedral occupancy by Fe³⁺ takes place
19 in both dioctahedral and trioctahedral 2:1 phyllosilicates. The partition coefficient approach
20 (Decarreau and Petit, 2014) while focusing on distribution of Al³⁺ and Fe³⁺ between octahedral
21 and tetrahedral sites of dioctahedral smectites has been disregarded in the Cuadros et al. (2019)'s
22 study. This approach was applied here on the Cuadros et al. (2019)'s set of data. The partition
23 coefficient value linked to the distribution of Al³⁺ and Fe³⁺ between octahedral and tetrahedral
24 sites determined from natural and synthetic dioctahedral smectites applies well to trioctahedral
25 phyllosilicates too. Data from synthetic iron-rich 2:1 smectites fit also well with both Cuadros et
26 al. (2019) and Decarreau and Petit (2014) models.

27

28 **Keywords:** 2:1 phyllosilicates, tetrahedral Fe, partition coefficient, smectite, nontronite.

29

30
31
32 Cuadros et al. (2019) used a wide range of data (70 samples) concerning dioctahedral and
33 trioctahedral Fe³⁺-bearing 2:1 phyllosilicates, to propose a model describing how tetrahedral
34 occupancy by Fe³⁺ takes place in both dioctahedral and trioctahedral 2:1 phyllosilicates. The data
35 came from the investigation of 2:1 phyllosilicates of submarine hydrothermal origin (29) and
36 from literature (41).

37 Cuadros et al. (2019) wrote: “With respect to *cation competition* for specific sites in
38 phyllosilicates, it appears that the radius and charge of Si⁴⁺, Al³⁺, Fe³⁺, Fe²⁺, and Mg²⁺ only allow
39 Al³⁺ and Fe³⁺ to occupy both tetrahedral and octahedral sites. The relative stability of these two
40 cations in the two sites should be a control for Fe(III) distribution between both sites”. On the
41 basis of this largely accepted assumption, and using the formalism for intra-crystalline
42 homovalent ions exchange between two nonequivalent sites, Decarreau and Petit (2014) proposed
43 a preexisting model based on a partition coefficient approach contradicting Cuadros et al.
44 (2019)’s claim to report for the first time a model of Fe³⁺ distribution in 2:1 phyllosilicates.
45 Decarreau and Petit (2014) showed that the distribution of Al³⁺ and Fe³⁺ between octahedral and
46 tetrahedral sites of dioctahedral smectites was controlled by a partition coefficient $K_{d(4/6)} =$
47 $[\text{Fe}^{3+}_4 * \text{Al}^{3+}_6] / [\text{Fe}^{3+}_6 * \text{Al}^{3+}_4]$, ($\text{Fe}^{3+}_4 = \text{Fe}^{3+} / (\text{Fe}^{3+} + \text{Al}^{3+})$) molar ratio in tetrahedra, 4 and 6
48 referring to tetrahedral and octahedral sites; similar relations for Al³⁺), and a $K_{d(4/6)}$ value of
49 0.006 was obtained from the fit of data from natural smectites formed at low temperature. This
50 very low $K_{d(4/6)}$ value was consistent with the physical model of Brice (1975), widely used for
51 the partitioning of elements in geochemistry. The model of Brice (1975) also predicts an increase
52 in $K_{d(4/6)}$ with the increase of temperature of mineral formation. Accordingly, a $K_{d(4/6)}$ value of
53 0.02 was measured from synthesis experiments of dioctahedral smectites at 200°C (Decarreau

54 and Petit, 2014). All data of Cuadros et al. (2019) (supplementary file S1) were plotted on a
55 classical geochemical diagram (Fe^{3+}_4 vs Fe^{3+}_6) to evaluate a Kd value (Fig. 1). Most of the data
56 are consistent with $\text{Kd}_{(4/6)}$ values ranging from 0.006 to 0.02 except two trioctahedral samples
57 (ferriphlogopite with no Al^{3+}_6 and talc/smectite with almost no Fe^{3+}_6 and Al^{3+}_6) and three
58 nontronites (HQ and two NG1 with different structural formulae). The partition coefficient
59 approach of Decarreau and Petit (2014), established for dioctahedral smectites, appears efficient
60 for a large variety of both di- and tri-octahedral 2:1 phyllosilicates. A single $\text{Kd}_{(4/6)}$ value suits to
61 most samples irrespective of their di- or tri-octahedral character and of their amount of M^{2+}
62 (Fig.1).

63 It is possible to evaluate the amount of tetrahedral Fe^{3+} from the total amount of Fe^{3+} and the
64 $\text{Kd}_{(4/6)}$ value determined by Decarreau and Petit (2014), fixing the amount of octahedral M^{2+}
65 cations and the layer charge. The Cuadros et al (2019)'s data of figure 1 were reported on figure
66 2. Most of di- and tri-octahedral samples fit well using a $\text{Kd}_{(4/6)}$ value of 0.006, a tetrahedral
67 charge of 1, and an amount of M^{2+} cations from 0.2 to 0.8 (for $\text{O}_{20}(\text{OH})_4$) (Fig.2). The
68 trioctahedral samples that are out of the range are micas and Fe-rich saponites with none or very-
69 low total amount of Al. Nevertheless, the data are consistent with a low $\text{Kd}_{(4/6)}$ value (Fig.2).

70 For the selection of literature data, Cuadros et al. (2019) disregarded some relevant data
71 concerning micas (Semenova et al., 1984) and excluded some data from synthetic nontronites
72 (Petit et al., 2015; Baron et al., 2016) because tetrahedral Fe^{3+} was mainly obtained using IR
73 spectroscopy. Due to their high total Fe^{3+} and high Fe^{3+}_4 amounts compared to natural samples,
74 the series of well characterized synthetic nontronites are interesting samples to study iron status
75 in clay minerals (Petit et al., 2017). Several studies gave strong evidence that the wavenumber of
76 several IR bands, and notably the main Si-O band at about 1000 cm^{-1} can be used efficiently to
77 quantify the octahedral and tetrahedral Fe^{3+} amounts (Petit et al., 2015; Baron et al., 2016). These

78 samples of Baron et al. (2016) were also studied by chemical analysis using scanning electron
79 microscope equipped with an energy dispersive spectrometer, Mössbauer spectroscopy (Baron et
80 al., 2017), and by X-ray diffraction that supported well the IR results. Cuadros et al. (2019)
81 alleged that these data from synthetic nontronites fit their regression. Why thus exclude these data
82 for their study?

83

84

REFERENCES

85

86 Baron, F., Petit, S., Tertre, E., and Decarreau, A. (2016) Influence of aqueous Si and Fe
87 speciation on tetrahedral Fe (III) substitutions in nontronites: a clay synthesis approach. *Clays
88 and Clay Minerals*, 64, 230–244.

89 Baron, F., Petit, S., Pentrák, M., Decarreau, A., and Stucki, J. W. (2017) Revisiting the nontronite
90 Mössbauer spectra. *American Mineralogist*, 102, 1501–1515.

91 Brice J.C. (1975) Some thermodynamic aspects of the growth of strained crystals. *Journal of
92 Crystal Growth*, 28, 249-283.

93

94 Cuadros, J., Michalski, J. R., Darby Dyar, M., and Dekov, V. (2019) Controls on tetrahedral Fe
95 (III) abundance in 2:1 phyllosilicates. *American Mineralogist*, 104, 1608–1619.

96

97 Decarreau, A., and Petit, S. (2014) Fe³⁺/Al³⁺ partitioning between tetrahedral and octahedral sites
98 in dioctahedral smectites. *Clay Minerals*, 49, 657-665.

99

100 Petit, S., Decarreau, A., Gates, W., Andrieux, P., and Grauby, O. (2015) Hydrothermal synthesis
101 of dioctahedral smectites: The Al-Fe³⁺ chemical series. Part II: Crystal-chemistry. *Applied Clay
102 Science*, 104, 96–105.

103

104 Petit, S., Baron, F., and Decarreau, A. (2017) Synthesis of nontronite and other Fe-rich smectites:
105 a critical review. *Clay Minerals*, 52, 469–483.

106

107 Semenova, T.F., Rozhdestvenskaya, I.V., and Frank-Kamenetskii, V.A. (1984) The structural
108 characteristics of micas with tetrahedral iron content regarding isomorphous substitutions. *Acta
109 Crystallographica*, A40, C257-C258.

110

111

112

Figure captions

113

114 **Figure 1:** Plot of Fe^{3+}_4 vs Fe^{3+}_6 molar ratio (see text). Squares: dioctahedral phyllosilicates;
115 triangles: trioctahedral phyllosilicates. Open symbols: outlying data (see text). Red curve: Fe^{3+}_4
116 vs Fe^{3+}_6 values in the case of a partition coefficient $\text{Kd}_{(4/6)} = 0.006$; green curve: Fe^{3+}_4 vs Fe^{3+}_6
117 values in the case of a partition coefficient $\text{Kd}_{(4/6)} = 0.02$.

118
119 **Figure 2:** Plot of Fe^{3+}_4 vs total Fe^{3+} (for $\text{O}_{20}(\text{OH})_4$). Squares: dioctahedral phyllosilicates;
120 triangles: trioctahedral phyllosilicates. Open symbols: outlying data (dioctahedral data in Fig. 1);
121 Curves were calculated with $\text{Kd}_{(4/6)} = 0.006$. Blue curve: $\text{M}^{2+} = 0.2$ and tetrahedral charge = 1;
122 green curve: $\text{M}^{2+} = 0.8$ and tetrahedral charge = 1; violet curve: $\text{M}^{2+} = 3$ and tetrahedral charge =
123 1; red curve: $\text{M}^{2+} = 3.85$ and tetrahedral charge = 2.

124

Figure 1

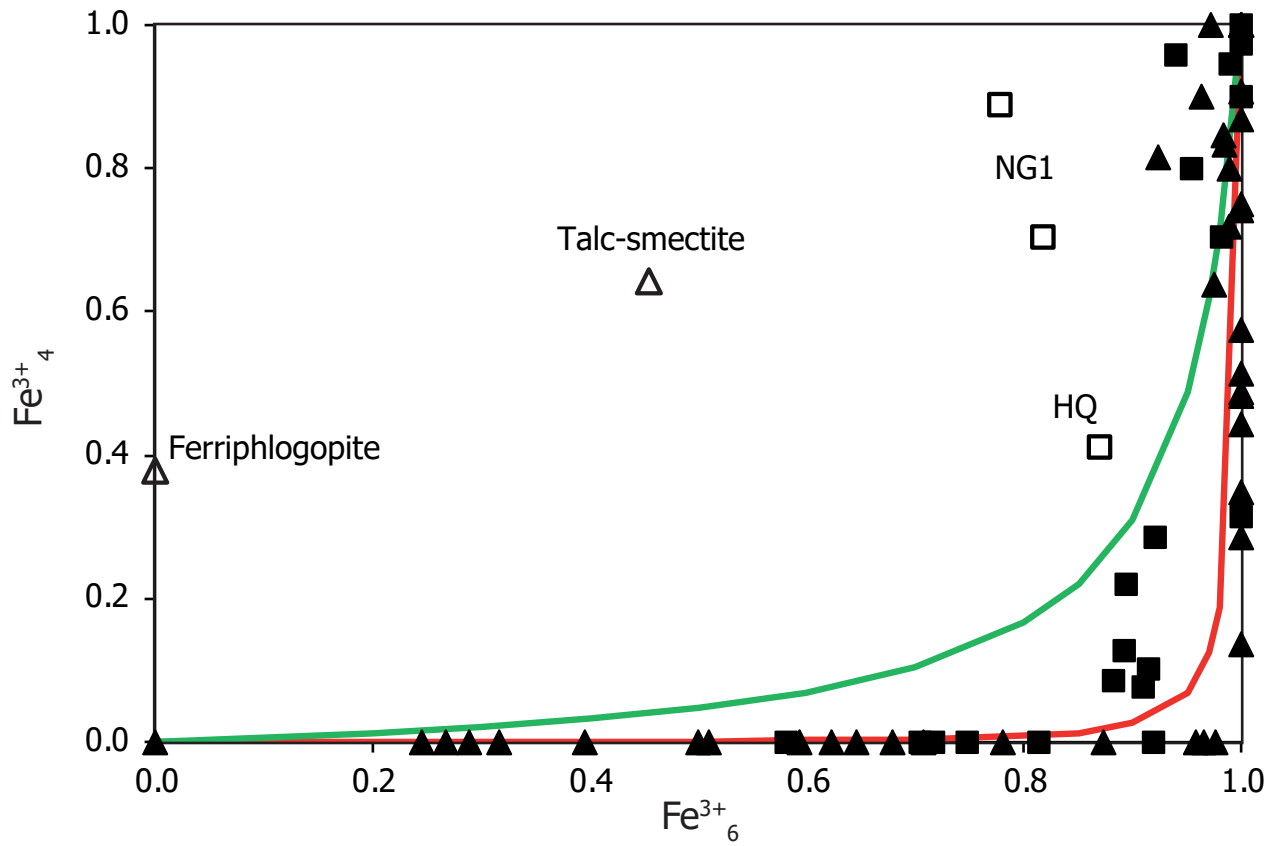


Figure 2

